

# Evolution of magnetic bubble domains in the uniaxial ferromagnet CeRu<sub>2</sub>Ga<sub>2</sub>B inferred from the Hall effect and ac magnetic susceptibility

Peter E. Siegfried<sup>†,1</sup>, Mark Maus<sup>‡,1</sup>, Alexander C. Bornstein<sup>§,1</sup>, Dirk Wulferding<sup>2</sup>, Jeehoon Kim,<sup>3</sup> Ryan E. Baumbach,<sup>4</sup> Eric D. Bauer,<sup>5</sup> Filip Ronning,<sup>5</sup> and Minhyea Lee<sup>1</sup>

<sup>1</sup>*Department of Physics, University of Colorado, Boulder, CO 80309, USA*

<sup>2</sup>*Department of Physics and Astronomy, Sejong University, Seoul, South Korea*

<sup>3</sup>*Department of Physics, POSTECH, Pohang, South Korea*

<sup>4</sup>*Physics Department, University of California Santa Cruz, Santa Cruz, CA 95064, USA*

<sup>5</sup>*Los Alamos National Laboratory, Los Alamos, New Mexico 87545, USA*

(Dated: August 25, 2025)

We study the Hall effect, AC magnetic susceptibility ( $\chi_{ac}$ ), and magnetic force microscopy (MFM) of the uniaxial ferromagnet CeRu<sub>2</sub>Ga<sub>2</sub>B with a centrosymmetric crystal structure. We observe a finite topological Hall effect (THE) within the ordered phase before the magnetization is polarized by applied field. By comparing the field dependences of the area fraction of the magnetic bubbles, the derivative of  $\chi_{ac}$ , and the THE signal, we deduce that the magnetic bubbles in CeRu<sub>2</sub>Ga<sub>2</sub>B evolve from the trivial to topological spin texture with field. Our findings will be utilized to expand the search for magnetic materials hosting the topological spin textures to ones with uniaxial anisotropy, and open a new possibility to tailor the topological spin texture.

## I. INTRODUCTION

Intermetallic  $f$ -magnetic materials have long been of central interest as they host a wide range of fascinating magnetic phases, including complex local moment order [1–3], nonFermi-liquid behavior [4], hidden ordered states [5, 6] and superconductivity adjacent to the magnetic phases [7]. The complex interplay between the lattice, charge, orbital, and spin degrees of freedom often are mediated by a variety of interaction channels such as Ruderman-Kittel-Kasuya-Yoshida (RKKY) interaction [8–10], crystal electric field splitting [11, 12], and the Kondo interaction [13, 14].

Recently, there has been a surge of interest in a new group of centrosymmetric lanthanide intermetallics that host the Skyrmion states [15–17] or non-trivial spin texture inferred from other physical quantities [18, 19]. In these materials, instead of a Dzyaloshinskii-Moriya interaction (DMI), competition among strong anisotropy, magnetic dipole-dipole interaction and Zeeman energy play a crucial role in stabilizing non-trivial spin texture [20, 21]. This is contrasted with extensive studies of so-called B20 materials such as MnSi [22], Fe<sub>0.5</sub>Co<sub>0.5</sub>Si [23] and FeGe,[24], where the non-centrosymmetric crystal structure enables a competition between ferromagnetism and DMI resulting in non-collinear and non-coplanar spin textures like the Skyrmion lattice [25, 26].

Another example of a region with non-collinear spin textures is a magnetic bubble, which refers to a circular-shaped region in which the enclosed spins point in different directions from the surrounding area. This includes magnetic vortices and domain walls. Magnetic bubbles have been a familiar concept in nano- and micro-scale magnetism for many decades [27]. The formation of bubble-like domains typically occurs in strong uniaxial magnets, as it balances the magnetic dipole interaction among domains and anisotropy. The discovery of a

magnetic Skyrmion lattice phase in MnSi [22] renewed great interest in these topological defects in magnetic systems thanks to their spectacular dynamical properties and emergent electromagnetic phenomena that offer great potential for novel magnetic storage and other spintronics applications [26, 28, 29].

CeRu<sub>2</sub>Ga<sub>2</sub>B is a centrosymmetric metallic ferromagnet with a Curie temperature  $T_C = 15.5$  K, where the local moments from Ce  $4f$ -electrons order without significant hybridization with the conduction electron state [30]. It exhibits highly uniaxial magnetic anisotropy with the magnetic easy axis along the  $c$ -axis, where a small applied field ( $H_S = 0.15$  T) brings the system to the spin-polarized state, while the same magnitude of field applied in the  $ab$  plane barely induces any magnetization [Fig. 1(a)]. The strong Ising-like anisotropy is thought to originate from the crystal electric field effect of Ce<sup>3+</sup> single ion anisotropy. [31, 32].

Previously, magnetic bubble domains on the  $ab$ -plane of CeRu<sub>2</sub>Ga<sub>2</sub>B were observed by Wulferding *et al.* [33], via magnetic force microscopy (MFM) under applied field along the  $c$ -axis below  $T_C$ . The bubble-like domains are observed unambiguously in MFM due to its superb sensitivity to changes in the out-of-plane components of magnetization: however, the limited spatial resolution of the MFM makes it hard to reveal the local spin configuration within a bubble to determine so-called topological charge ( $\mathcal{N}$ ), which refers to the number that counts how many times the arrows of spin directions within the structure wrap around a sphere [25, 26]:

$$\mathcal{N} = \frac{1}{4\pi} \oint_{\mathcal{A}} \mathbf{n} \cdot \left( \frac{\partial \mathbf{n}}{\partial x} \times \frac{\partial \mathbf{n}}{\partial y} \right) dx dy, \quad (1)$$

where  $\mathcal{A}$  is the area of a bubble, and  $\mathbf{n}(\mathbf{r})$  denotes the directions of spins at a position  $\mathbf{r}$ .

If a spin texture extended to macroscopic length scales contains these bubbles with non-zero topological charge

(e.g.  $\mathcal{N} = 1$  for a Skyrmion), it should lead to a macroscopic electromagnetic response associated [21, 26, 34]. These includes but not limited to the topological Hall effect (THE) [35–37], magnetic AC susceptibility [38, 39], specific heat [40] and magnetoresistance [41, 42] similar to what was observed in the Skyrmion lattice phase.

In this paper, we present the field ( $H$ ) and temperature ( $T$ ) dependence of the topological Hall resistivity ( $\rho_{xy}^T$ ) as well as ac magnetic susceptibility ( $\chi_{ac}$ ) of ordered phase of  $\text{CeRu}_2\text{Ga}_2\text{B}$  ( $T < T_C$ ). We trace the variation of the topological charge using  $\rho_{xy}^T$  as a gauge by comparing it to the area fraction change of bubble domains observed in MFM as a function of field. At a fixed  $T$ ,  $\rho_{xy}^T$  reaches its maximum at  $H = H_T$ , which is narrowly apart from another field scale  $H_P$ , where the derivatives of  $\chi_{ac}$  with respect to field ( $\frac{d\chi_{ac}}{dH}$ ) exhibit the maximum magnitude. This is similar to what was observed in B20 magnet  $\text{MnSi}$ , where  $\chi_{ac}(H)$  exhibits a step-like change and  $\frac{d\chi_{ac}}{dH}$  a delta function [38, 39] upon the formation of the Skyrmion Lattice. Meanwhile such change in  $\text{CeRu}_2\text{Ga}_2\text{B}$  appears with large broadening. We also find that the area fraction of the bubble remains constant in  $H < H_T$ , but decreases rapidly as the field is increased further, in the same manner as the THE signal does.

Based on our observation, we speculate the magnetic bubble in  $\text{CeRu}_2\text{Ga}_2\text{B}$  undergoes the following evolution with field: it begins as a trivial magnetic domain with zero topological charge in zero field. As the field increases, the topological charge within a bubble appears to lead to a finite  $\rho_{xy}^T$  signal, which goes back to zero as getting close to the saturation field. Furthermore, based on the analogy to the behavior of  $\frac{d\chi_{ac}}{dH}$  in B20 magnet [38, 39, 43], the broad peak in  $\frac{d\chi_{ac}}{dH}(H)$  indicates the wide variation of the onset field values for the topological charge to emerge in individual magnetic bubbles in  $\text{CeRu}_2\text{Ga}_2\text{B}$ .

Our findings will be utilized to expand the search of magnetic materials hosting the topological spin textures to ones with uniaxial anisotropy, and open a new avenue to tailoring topological defects in magnetic thin films, of which the coplanar magnetic bubbles are ubiquitously observed but topological ones are less common [44–47].

## II. EXPERIMENTAL METHODS

Single crystals of  $\text{CeRu}_2\text{Ga}_2\text{B}$  were grown by the Czochralski method [30] Magnetization ( $M$ ) data were measured using a Quantum Design magnetic properties measurement system. Magneto transport measurements were performed in a standard Hall-bar geometry, where the contact was made using Dupont Ag paints with a typical contact resistance of  $\leq 1 \Omega$ . The sample sizes range  $1\text{--}2 \times 0.5\text{--}1 \times 0.5\text{--}1 \text{ mm}^3$ . All the magneto transport data are obtained in the applied magnetic field along the crystalline  $c$ -axis and the DC current of 2 – 6 mA was flown within the  $ab$ -plane. The magnetic field was generated

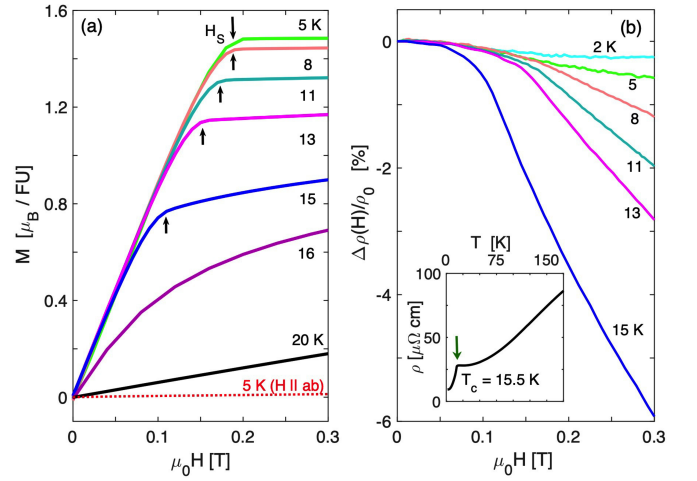


FIG. 1. (a) Magnetization as a function of applied magnetic field  $H$  in  $\mathbf{H} \parallel c$  at different temperatures. The saturation of  $M(H)$  at  $H_S$  is indicated for each temperature (black arrow) and  $H_S$  decreases as  $T$  approaches  $T_C = 15.5$  K. The magnitude of  $M$  for  $\mathbf{H} \parallel ab$  is minuscule (dotted line), compared to  $\mathbf{H} \parallel c$ . (b) The fractional MR at various temperatures is shown as a function of  $H$ . Below  $T_C$ , MR changes little in  $H < H_S$ . The inset shows the zero field resistivity, where  $T_C$  is clearly marked (arrow) by the rapid drop in resistivity with decreasing temperature.

by the 7 T superconducting magnet sitting in the liquid Helium bath.

The ac magnetic susceptibility measurements were performed with a home-built nesting coil set, which comprises a driving coil to generate a very small ac magnetic field and a pair of pick-up coils, coaxially placed within the driving coil. The two pick-up coils are wound in opposite directions and connected in series to ensure equal mutual inductance with opposite sign. This results in zero net induced voltage in a null state. When the sample is placed in only one of the pick-up coils, a nonzero net voltage is induced, the magnitude of which is directly proportional to the change of magnetic flux contributed by the sample. This voltage is measured with a digital lock-in at a driving frequency and amplitude of 997 Hz and 7.1 gauss. Heat sinking for the sample inside the coil was achieved by adhering the samples to the long, thin sapphire rod using GE varnish. This rod is then inserted through the pick-up coils and anchored to the cold finger. The crystalline  $c$ -axis is aligned to the co-axis of the pick-up and driving coils that are parallel to the applied DC field. We find the background signal of coils is negligible compared to the signal generated by the presence of the samples.

MFM images were taken with a home-built MFM probe inside a cryostat with superconducting magnets. Details of the setup are described elsewhere [33, 47, 48].

For the rest of this article, the applied magnetic field direction is always parallel to the crystalline  $c$ -axis,  $\mathbf{H} \parallel c$ , unless otherwise specified.

### III. RESULTS AND DISCUSSION

Fig. 1(a) displays the magnetization ( $M$ ) of  $\text{CeRu}_2\text{Ga}_2\text{B}$  as a function of field along the  $c$ -axis at various temperatures. A saturated moment of  $1.55\mu_B$  per Ce is reached at  $\mu_0 H_S \simeq 0.18$  T and remains constant up to  $\mu_0 H = 7$  T, at  $T = 5$  K. The saturation field  $H_S$ , marked by arrows, decreases as  $T$  gets close to  $T_C$ . The linear increase of  $M_C$  up to the finite  $H_S$  indicates the slow polarization of abundant magnetic domains in the zero field (ZF) state. We find that the magnetization in  $\mathbf{H} \parallel ab$  is two orders of magnitude smaller than  $M$ , which highlights the strong uniaxial magnetic anisotropy of the system. Fig. 1(b) shows the fractional MR (fMR), defined as  $\Delta\rho(H)/\rho_0 = [\rho(H) - \rho_0]/\rho_0$ , where  $\rho$  refers to the longitudinal resistivity, and  $\rho_0 = \rho(H = 0)$  at a given  $T$ , as shown in the inset. The fMR is always negative and its magnitude ranges a few % in  $H < H_S$  below  $T_C$ . Changes in MR for  $H > H_S$  become more obvious once  $T$  increases close to  $T_C$ , due to the effective reduction of spin scattering with the conduction electrons in the fully polarized local spin state in  $H > H_S$ . A sharp drop in the  $\rho$  vs  $T$  plot, shown in the inset and marked by a green arrow, confirms the reduced spin scattering upon ordering.

Next, we show the Hall resistivity ( $\rho_{xy}$ ) of  $\text{CeRu}_2\text{Ga}_2\text{B}$  as a function of applied field in Fig. 2(a) at  $T = 2, 5, 8, 11, 13, 15$  and 20 K. Similar to the  $M(H)$ , the saturation field  $H_S$  is clearly identifiable by the kink in  $\rho_{xy}(H)$ .

The ordinary Hall coefficient,  $R_H$  at a given  $T$  is obtained from the linear high-field slopes ( $H > H_S$  up to 7 T, not shown here).  $R_H$  is negative for all  $T$ , except for  $T = 20$  K at which  $\rho_{xy}(H)$  does not show the linear  $H$  dependence up to 7 T. The positive slope of  $\rho_{xy}$  at 20 K simply reflects the anomalous Hall signal ( $\rho_{xy}^A$ ) induced by field-induced magnetization, where the kink marking  $H_S$  below  $T_C$  has moved out to the higher field, leaving the AHE with the positive slope. This is commonly observed in ferromagnetic intermetallic systems [49].

In order to identify the different contributions to the Hall resistivity in  $T < T_C$ , first, we parse the  $\rho_{xy}(H)$  into the ordinary Hall contribution that is linear in  $H$  at high field ( $\mu_0 R_H H$ ) and the remainder of signal,  $\rho'_{xy}$  [50].  $\rho'_{xy}$  includes both the anomalous Hall resistivity  $\rho_{xy}^A$ , and the topological Hall effect (THE) contribution  $\rho_{xy}^T$ . The former is proportional to the overall magnetization, and the latter is attributed to the topological charge arising from non-spin texture within the magnetic bubbles.

$$\rho'_{xy}(H) = \rho_{xy}(H) - \mu_0 R_H H = \rho_{xy}^A + \rho_{xy}^T \quad (2)$$

When the  $H$ -linear ordinary Hall contribution ( $\mu_0 R_H H$ ) is subtracted from  $\rho_{xy}(H)$  to obtain  $\rho'_{xy}$  in  $\text{CeRu}_2\text{Ga}_2\text{B}$ , we find that  $\rho'_{xy}$  cannot be captured by the anomalous Hall effect (AHE) alone: The anomalous Hall resistivity ( $\rho_{xy}^A$ ) is proportional to  $M$  with the anomalous Hall coefficient  $R_S$  that is defined as  $\rho_{xy}^A = R_S M$ , with  $R_S$  being

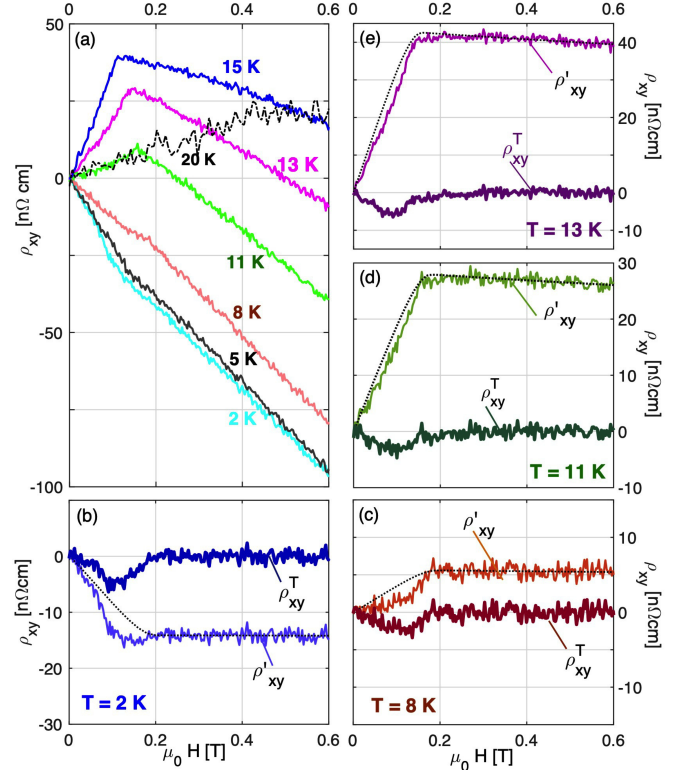


FIG. 2. (a)  $\rho_{xy}(H)$  measured at  $T = 2, 5, 8, 11, 13, 15$  and 20 K. (b-e) Separating out the THE ( $\rho_{xy}^T$ ) from  $\rho'_{xy} = \rho_{xy} - \mu_0 R_H H$  for (b)  $T = 2$  K, (c) 8 K, (d) 11 K, and (e) 13 K.  $\rho_{xy}^T(H)$  (darker, bold lines) is determined by subtracting  $\rho_{xy}^A(H) = S_H \rho^2 M$  (dotted lines) from  $\rho'_{xy}$  in each panel. See text for details.

a function of both  $H$  and  $T$ . As  $T$  increases, there is a change in the kink angle at  $H_S$  between  $T = 5$  and 8 K [Fig. 2 (a)], indicating the sign change of  $R_S$ .

We find at a given  $T$   $\rho_{xy}^A$  of  $\text{CeRu}_2\text{Ga}_2\text{B}$  is best described by  $\rho_{xy}^A = S_H \rho^2 M$ , where  $R_S$  is expressed with a  $H$ -independent constant  $S_H$  and  $\rho(H)$ , magneoresistance as shown in Fig. 1(b) [50]. It particularly captures better the subtle concave curvature of  $\rho'_{xy}$  in  $H > H_S$  than using  $R_S = A\rho$ , with  $A$  is a proportional constant. Dotted lines in panels Fig. 2 (b-e) display the best-fit results of  $\rho_{xy}^A = S_H \rho^2 M$ , at  $T = 2, 8, 11$  and 13 K.

After carefully characterizing the anomalous Hall contribution, we can finally extract the topological Hall contribution from the differences between  $\rho'_{xy}$  and  $\rho_{xy}^A$  according to Eq. 2 [35, 36, 51].  $\rho_{xy}^T(H)$  of  $\text{CeRu}_2\text{Ga}_2\text{B}$  at each  $T$ 's is shown in the thicker lines in the panels (b-e). The finite  $\rho_{xy}^T$  values exhibit similar  $H$ -profiles at all temperatures: it starts from zero to increase smoothly with  $H$  and reaches its maximum value at  $H = H_T$  before decreasing back to zero as  $H \rightarrow H_S$ . We infer from this non-monotonic behavior of  $\rho_{xy}^T$  that  $\text{CeRu}_2\text{Ga}_2\text{B}$  hosts the non-trivial spin texture that enables the finite THE signal upon applying magnetic field, but the onset field of

such a texture may be broadly distributed across a range of field as  $\rho_{xy}^T$  rises smoothly with field. We note that the disappearance rate of  $\rho_{xy}^T$  near  $H_S$  is faster than the appearance rate near ZF throughout all temperatures, indicating that the onset field of transition into the topological spin textures may have a larger distribution than the field of the spin polarization field scale. We will come back and discuss this further in Fig. 4.

While  $\rho_{xy}^A(H)$  mostly follows the  $H$ -profile of the magnetization – monotonically increasing with  $H$  and then saturating. The sign change in  $S_H$  between 5 and 8 K is obvious by flipping  $\rho_{xy}$  with respect to the horizontal axis. Meanwhile, the field dependence of  $\rho_{xy}^T$  exhibits a clear maximum at  $H = H_T$ , which varies slightly with  $T$  and the sign remains negative throughout. Table 1 lists  $R_H$  and  $S_H$  and the maximum value of  $\rho_{xy}^T$  at each temperature.

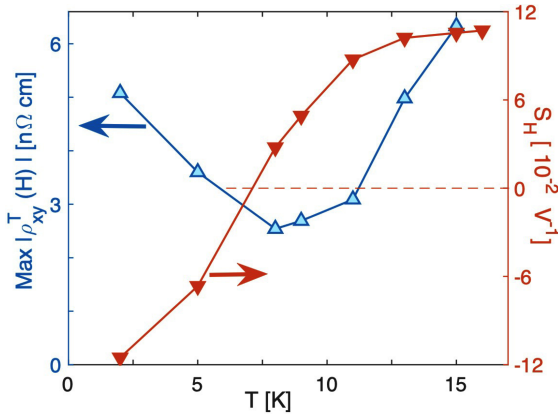


FIG. 3. Temperature dependence of the maximum magnitude of  $|\rho_{xy}^T(H)|$  (left  $y$ -axis) and  $S_H$  (right  $y$ -axis). The sign of  $S_H$  changes from negative to positive between 5 and 8 K, while that of  $\rho_{xy}^T$  remains negative.

In Fig. 3, we plot  $S_H$  (right  $y$ -axis) and the maximum value of  $|\rho_{xy}^T|$  (left  $y$ -axis) as a function of  $T$ . The sign of  $S_H$  changes from negative to positive between 5 and 8 K, while that of  $\rho_{xy}^T$  remains negative. It is interesting to compare the sign change of  $S_H$  to that of Fe-doped MnSi samples. In  $\text{Mn}_{1-x}\text{Fe}_x\text{Si}$ , it was found that the sign of the THE remains the same [52], while that of  $S_H$  depends on the Fe doping level. This is expected because the origin of the sign of AHE is more complex, involving material-specific traits such as electronic wave function leading to the Berry curvature, spin-orbit coupling and the level of disorders [53]. On the other hand, the THE sign is set by the real space spin texture, e.g., the handedness of Skyrmions and hence remains the same as long as the normal Hall coefficient remains the same [52, 54–56].

The finite THE signal with non-monotonic field dependence below  $H_S$  indicates that  $\text{CeRu}_2\text{Ga}_2\text{B}$  hosts a non-trivial (i.e. non-collinear and non-coplanar) spin texture that supports the topological charge as expressed in Eq. (1). Hence, we hypothesize that the topological Hall

contribution in  $\text{CeRu}_2\text{Ga}_2\text{B}$  should originate from the magnetic bubbles observed in MFM images [33] and that the spin texture within a bubble evolves with increasing field from zero.

To further examine this hypothesis, we investigate the magnetic AC susceptibility, which has been demonstrated to exhibit high sensitivity upon the transitions to the Skyrmion lattice [38, 39].

Fig. 4(a) displays the  $H$  dependence of  $\chi_{ac}$ , and (b) its derivative ( $\frac{d\chi_{ac}}{dH}$ ) that is normalized by the maximum value of  $\frac{d\chi_{ac}}{dH}$  at each  $T$ . Despite nearly linear relation between  $M$  and  $H$  [Fig. 1(a)],  $\chi_{ac} (\propto \frac{dM}{dH})$  shows a considerable  $H$  dependence, far from constant, at all measured temperatures. Knowing that  $\chi_{ac}$  is highly sensitive to a change of the spin stiffness, this implies the realignment of spin texture within domains with field occurs in a more complex manner than what appears in the gradual increase of magnetization.

To understand better, we take the derivatives of  $\chi_{ac}(H)$  with respect to  $H$  and plot its absolute values in Fig. 4(b):  $|\frac{d\chi_{ac}}{dH}|$  starts at a finite value at zero field (ZF) in  $T < 11$  K, which decreases to zero in higher temperatures. At all temperatures it exhibits a broad peak with its maximum occurring at  $H = H_P$  as marked with arrows.  $H_P$  decreases slowly with increasing  $T$  and the slow change rate at lower  $T$ 's reflects the higher spin stiffness.

Here, we point out the similarity between our  $\chi_{ac}(H)$  data in  $\text{CeRu}_2\text{Ga}_2\text{B}$  and that of B20-type helimagnets, such as MnSi [38, 39], Fe-doped MnSi [57] and FeGe [43]: upon entering the Skyrmion lattice, at a given temperature,  $\chi_{ac}$  vs  $H$  of B20 magnets exhibits a step-like change and  $\frac{d\chi_{ac}}{dH}$  displays delta-function-like behavior. Because a Skyrmion lattice in these B20 helimagnets forms a high symmetry long-range pattern, it is not surprising to leave unambiguous thermodynamic signatures in  $\chi_{ac}$  as well as specific heat [40, 57] to mark the transition field from the trivial to topological spin textures.

On the other hand, such a transition in the bubble-like

TABLE 1. Fitting parameters used in parsing the different contributions of the Hall signal,  $\rho_{xy}(H) = \mu_0 R_H H + S_H \rho^2 M + \rho_{xy}^T$ , where  $R_H$  and  $S_H$  are  $H$ -independent constants at a given  $T$ .

| $T$<br>[K] | $R_H$<br>[ $10^{-9} \text{ m}^3/\text{C}$ ] | $S_H$<br>[ $10^{-2} \text{ V}^{-1}$ ] | $\max  \rho_{xy}^T $<br>[ $\text{n}\Omega \text{ cm}$ ] |
|------------|---------------------------------------------|---------------------------------------|---------------------------------------------------------|
| 2          | -1.39                                       | -11.52                                | 5.08                                                    |
| 5          | -1.44                                       | -6.66                                 | 3.60                                                    |
| 8          | -1.41                                       | 2.77                                  | 2.54                                                    |
| 9          | -1.33                                       | 4.91                                  | 2.69                                                    |
| 11         | -1.08                                       | 8.75                                  | 3.09                                                    |
| 13         | -0.79                                       | 10.22                                 | 4.98                                                    |
| 15         | -0.50                                       | 10.56                                 | 6.33                                                    |
| 16         | -0.57                                       | 10.72                                 | N/A                                                     |



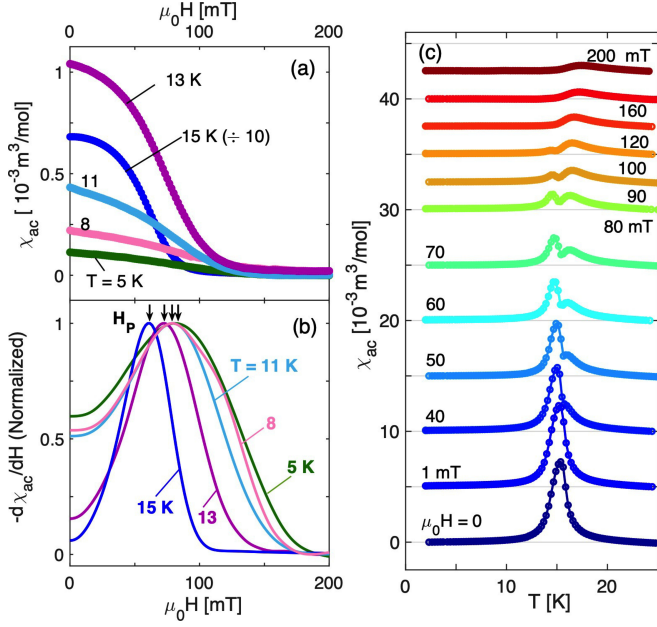


FIG. 4. (a)  $\chi_{ac}$  plotted as a function of  $H$ . Note that  $\chi_{ac}(H)$  at  $T = 15$  K is scaled by  $1/10$  in order to fit within the same range. (b) Derivative of  $\chi_{ac}$  as a function of  $H$ , normalized by the maximum value at each  $T$ . Vertical arrows mark the location of the peak in  $\frac{d\chi_{ac}}{dH}$ ,  $H_P$ . (c)  $T$  dependence of  $\chi_{ac}$  at fixed  $H$ . Each curve is displayed with an offset for clarity.

magnetic domains of  $\text{CeRu}_2\text{Ga}_2\text{B}$  are not expected to be sharp, because the individual bubbles may have different field scale transforming from the trivial to topological spin texture. Magnetic bubbles were observed even at zero field [33], which, we speculate, evolve smoothly from e.g. a coplanar magnetic vortice-like texture to ones with the finite topological charge. This evolution may happen at different fields for different domains. Hence, the clear maximum of  $\frac{d\chi_{ac}}{dH}(H)$  of  $\text{CeRu}_2\text{Ga}_2\text{B}$  is thought to be a broadened version of the delta function with a large width.

This broadening is attributed to two main distinctions from the B20 materials: First, unlike a Skyrmion lattice, the magnetic domains in  $\text{CeRu}_2\text{Ga}_2\text{B}$  do not have a long-range translational order as seen in the oxide films [44–46]. Second, the trivial-to-non-trivial spin texture transition occurs across a range of fields for different bubble domains, instead of having a sharp, well-defined value. We will discuss this more with the MFM data in Fig. 5.

Fig. 4(c) displays the  $T$  dependence of  $\chi_{ac}$  taken at constant fields as shown. The diverging magnitude of  $\chi_{ac}$  as  $T$  approaches  $T_C$  across  $T_C$  marks the long range magnetic ordering, consistent with the data shown in Fig. 4(a). We note that the peak of  $\chi_{ac}(T)$  near  $T_C$  begins to split at an applied field of  $\mu_0 H = 40$  mT with a pronounced splitting observed at  $\mu_0 H = 50$  mT. The peak at lower temperature is situated at  $T = 14.9$  K for 50 mT and changes to 14.3 K at 120 mT. Meanwhile, the high  $T$  peak starts to emerge at  $T = 16.1$  K at  $\mu_0 H = 50$

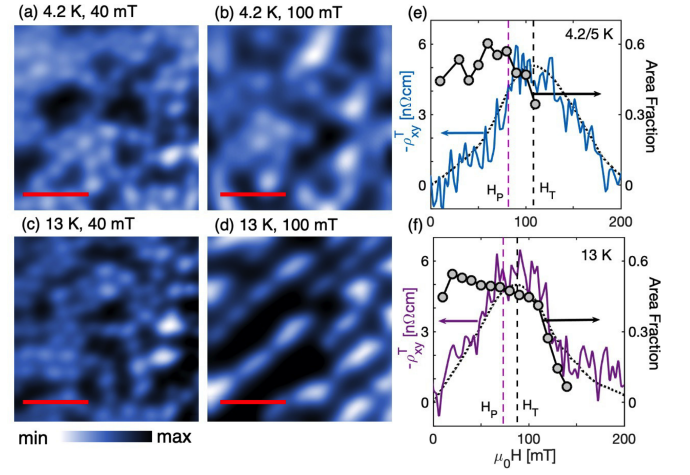


FIG. 5. MFM images at  $\mu_0 H = 40$  (left) and  $100$  mT (right) at  $T = 4.2$  K (a, b) and at  $T = 13$  K (c, d) with the scan area  $14 \times 14 \mu\text{m}^2$ . All images were taken with initially field-cooled at  $\mu_0 H = 10$  mT. Scale bar corresponds to  $5 \mu\text{m}$ . The colorbar indicates the linear scale between the minimum and maximum frequency shifts of the cantilever at each  $T$ . (e)  $\rho_{xy}^T(H)$  (solid line, left  $y$ -axis) and area fraction of the bubble-like domains (gray circles, right  $y$ -axis) at  $T = 4.2$  K as a function of  $H$  and (f) at  $13$  K. Dotted lines are a guide for the eyes for  $\rho_{xy}^T$ .  $H_P$  and  $H_T$  are marked with the vertical dashed lines, where the maximum of  $\frac{d\chi_{ac}}{dH}$  and  $\rho_{xy}^T(H)$  are found, respectively.

mT and moves to  $17.4$  K at  $200$  mT, where the lower peak becomes mostly invisible. We speculate that the emergence of two peaks at a finite field originates from robust pinning with an energy scale comparable to  $\approx k_B T_C$  and thus is likely to survive at elevated temperature [58].

We now turn to the MFM images to compare the area fraction of magnetic bubbles [59] and the magnitudes of the THE signals. In Figs. 5(a)-(d), we display the frequency shifts obtained in the same scanned area of  $14 \times 14 \mu\text{m}^2$  at  $\mu_0 H = 40$  and  $100$  mT, which correspond to below  $H_P$  and above  $H_T$ , respectively. The MFM images are taken after initial field-cooling through  $T_C$  at  $\mu_0 H = 10$  mT. Panels Fig. 5(e) and (f) show the  $H$  dependence of the magnitude of  $\rho_{xy}^T$  (left  $y$ -axes) and the area fraction (right  $y$ -axes) for  $T = 4.2$  and  $13$  K, respectively. At  $T = 4.2$  K, the bubble domains in circular shapes with diameters ranging from  $0.4$  to  $1 \mu\text{m}$  are distributed in the field of view, as shown in Fig. 5(a). The shape of the bubbles remains mostly circular until  $H$  reaches  $100$  mT at  $4.2$  K. However, at  $13$  K, the shape evolves from circular at low field [panel (c)] to rod-shaped at  $100$  mT [panel (d)]. The rod-shaped domains that appear only in the higher field, as seen in Fig. 5(d), act as precursors for the stripy domain walls that appear in the spin-polarized state in  $H > H_S$  [33]. Hence, they are more likely to appear at higher  $T$ s at a given field due to the reduced spin stiffness.

We define the area fraction as the ratio of the area oc-

cupied by bubbles over the scanned area. We plot the field dependence of the area fractions in comparison to that of  $\rho_{xy}^T$  in Fig. 5(e) and (f). At 4.2 K, it remains roughly constant at the value of  $0.5 \pm 0.1$  until  $H$  reaches  $H_T$ . Upon increasing  $H$  further, the area fraction begins to collapse between  $H_P$  and  $H_T$  [Fig. 5(e)]. At 13 K, the area fraction exhibits a similar value of 4.2 K with a small slope with field up to  $\mu_0 H = 100$  mT. As  $H$  increases further above  $H_T$ , shares a similar  $H$  dependence of  $\rho_{xy}^T$  of a rapid decline with field. The coincidence of the decline of the THE signal and the area fraction suggests that the bubbles with trivial (either collinear or coplanar or both) at low field have evolved to have non-zero topological charge that supports the finite THE signal. The limitations of MFM images – relatively large lateral resolution and the restricted sensitivity only to the out-of-plane spin component [60, 61] – prevents us from directly tracking such evolutions and hence results in little variation of the area fraction at low field. However, with the comparison of the THE, we infer a transformation of the internal spin texture of the magnetic bubble. The correlation between the bubble area fraction and the THE has been explored in other uniaxial magnetic thin films such as (Ca,Ce)MnO<sub>3</sub> [44] and La<sub>0.7</sub>Sr<sub>0.3</sub>Mn<sub>1-y</sub>Ru<sub>y</sub>O<sub>3</sub> [45].

This observation concurs with the hypothesis that the THE of CeRu<sub>2</sub>Ga<sub>2</sub>B is enabled by the magnetic bubbles with non-trivial texture present that is gradually developed with field. In other words, their total topological charges increase from zero at ZF and hit a maximum in the narrow range between  $H_P$  and  $H_T$  and then go back to zero as spin polarization sets in. The peak width of  $\frac{d\chi_{ac}}{dH}$  at  $H_P$  marks the wide distribution of the field scales for individual bubbles, at which the finite topological charge takes shape.

The next question is what the possible spin configurations would look like inside the trivial bubbles that do not contribute to the THE. The simplest arrangement would be either co-planar or collinear. Under the uniaxial anisotropy, there are two plausible geometries for such spin arrangements: The most straightforward one would be 180° (Ising-like) domain walls. Here, the characteristic wall width is proportional to  $\sqrt{A/K}$ , with  $A \simeq 2\pi M_S^2$  referring to the ferromagnetic exchange stiffness, and  $K$  being the magneto-crystalline anisotropy constant [62]. The condition of  $\mu_0 M_S^2/K \ll 1$  in the Ising-like magnet CeRu<sub>2</sub>Ga<sub>2</sub>B implies a relatively small domain width [44, 45], where the non-trivial spin texture may emerge along with the finite THE signal.

The other spin configuration consists of coplanar magnetic vortex cores [60, 63] with swirling patterns, *i.e.* non-collinear arrangement with a small out-of-plane component [60, 61, 63, 64]. This type has been historically referred to as a magnetic vortex with negligible or restricted out-of-plane components, which leads to invisibility to the MFM experiments. Upon increasing the field, they acquire the out-of-plane components aided by the uniaxial anisotropy, likely to evolve gradually to non-collinear and non-coplanar textures to have the finite

signal.

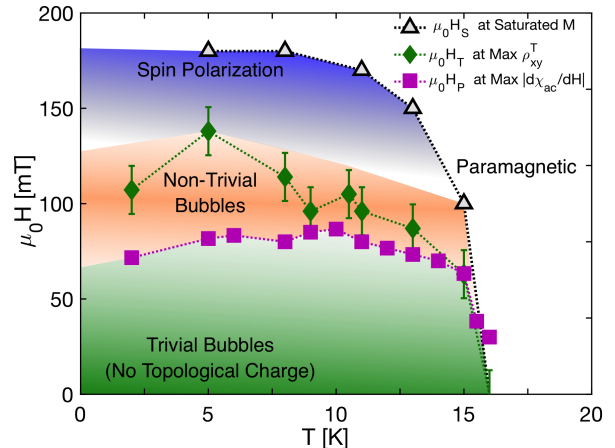


FIG. 6. Boundaries of spin structures within the ordered phase in CeRu<sub>2</sub>Ga<sub>2</sub>B in  $H$ - $T$  space. Three characteristic field scales observed in electrical and magnetic properties in  $T < T_C$ :  $H_P$  (square) refers to the field at the peak of  $\frac{d\chi_{ac}}{dH}$  ( $H$ ) [Fig. 4(b)],  $H_T$  (diamond) to the location of maximum magnitude of  $\rho_{xy}^T(H)$  [Fig. 3] and  $H_S$  (triangle) to the saturated magnetization [Fig. 1(a)].

Finally, we display the schematic phase diagram for the bubble domains as a function of  $H$  and  $T$  in Fig. 6, based on the field dependence of the area fractions and THE in CeRu<sub>2</sub>Ga<sub>2</sub>B. At zero field, bubbles are topologically trivial, but small fields induce nonzero topological charge with widely distributed onset scales. This is reflected in the gradual rise of THE and the broad width of  $\partial\chi/\partial H$  of which maximum fall into the close proximity to  $H_T$ . Near  $H_T$ , most bubbles transform to having topological texture, which MFM image do not have sensitivity to pick out this change, and thus the area fraction remains constant from zero field to approximately  $H_T$ . In  $H > H_T$ , the spin polarization starts and both area fraction and  $\rho_{xy}^T$  diminish jointly.

The phase diagram in Fig. 6 shows resemblance with the phase diagrams of Skyrmion systems with B20-structure [39, 41, 57]. The onset of the Skyrmion lattice phase boundary marked by the THE and  $\chi_{ac}$  in B20 systems is rather abrupt as a function of field, and it is independent of  $T$  [38, 41, 65]. Similarly, in CeRu<sub>2</sub>Ga<sub>2</sub>B, the representative field scales  $H_T$  and  $H_P$ , indicating the onset of the topological bubble domains, remain also mostly  $T$ -independent until very close to  $T_C$ , as shown in Fig. 6. However, the stark difference in CeRu<sub>2</sub>Ga<sub>2</sub>B is that the onset field to establish topological charge hugely varies bubble by bubble, thus the field dependence of the THE exhibit the gradual rise and fall. The size of the THE is also determined by the Skyrmion density, which is proportional to the effective gauge field responsible for generating the THE [52]. For CeRu<sub>2</sub>Ga<sub>2</sub>B, the large bubble size effectively reduces the magnitude of the gauge field, leading to the small magnitude of the THE signal as well.

#### IV. SUMMARY

We examine the field and temperature dependence of the THE signals and  $\chi_{ac}$  in the centrosymmetric  $\text{CeRu}_2\text{Ga}_2\text{B}$  with an Ising-like uniaxial anisotropy. We detect finite THE signals in  $2 < T < T_C = 15.5$  K. At a fixed  $T$ , starting from zero field,  $\rho_{xy}^T$  increases smoothly from zero upon increasing the field, having a maximum at  $H_T$  before decreasing to zero as  $H$  approaches the saturation field.  $\chi_{ac}(H)$  exhibits a smooth monotonic field dependence with  $|\frac{d\chi_{ac}}{dH}|$  displaying a broad peak with a maximum at  $H_P$ , which lies within close vicinity to  $H_T$ . By analogy with the behavior of  $\chi_{ac}(H)$  and  $\partial\chi/\partial H$  in B20 magnets, we interpret this as a gradual evolution of the spin texture within a magnetic bubble: topologically trivial magnetic bubbles at zero and low fields, which, with increasing field, transform into topological bubbles carrying nonzero topological charge and thereby contributing to the THE. Because of the limited sensitivity of magnetic force microscopy to in-plane moments, it may not capture this evolution, resulting in a constant bubble area fraction up to fields near  $H_P$  and  $H_T$ . However, for  $H > H_T$ , we observe the reduction in the are fraction caused by the spin-polarization follows the same field dependence as the THE. This correspondence indicates that most bubbles acquire topological charge near  $H_P$  and  $H_T$ , although the precise field at which this transformation occurs varies significantly from bubble to bubble, reflected in the broad peak in  $\frac{d\chi_{ac}}{dH}$ .

While a direct experimental probe of the spin configuration on a sub-micrometer length is not readily accessi-

ble for bulk crystals, our result establishes experimentally tangible signatures for the emergence of topological bubbles in the centrosymmetric, DMI-free magnets. It is expected to be widely applicable to searches for optimized materials that offer platforms for novel Skyrmion-based electronic devices.

#### ACKNOWLEDGMENTS

The work done in the University of Colorado Boulder was supported by the U.S. DOE, Basic Energy Sciences, Materials Sciences and Engineering Division under Award No. DE-SC0021377. J. K. was supported by the Ministry of Education, Science, and Technology (Nos. NRF-2016K1A4A01922028, NRF-2018R1A5A6075964, and NRF-2019R1A2C2090356). D.W. was supported by the faculty research fund of Sejong University in 2025. E.D.B. was supported by the U.S. DOE, Basic Energy Sciences, Materials Sciences and Engineering Division under the project ‘quantum fluctuations in narrow band systems’. F.R. was supported by the U.S. Department of Energy, Office of Science, National Quantum Information Science Research Centers, Quantum Science Center.

Current Address:

<sup>†</sup> Quantinuum, Broomfield, CO 80021

<sup>‡</sup> Department of Physics, University of California, Berkeley, CA 94720

<sup>§</sup> Analog Devices, Longmont CO 80501

- 
- [1] Kengo Fushiya, Tatsuma D. Matsuda, Ryuji Higashinaka, Kazuhiro Akiyama, and Yuji Aoki, “Possible existence of partially disordered sm ions in magnetically ordered state of ising magnet smpt2si2: A single crystal study,” *Journal of the Physical Society of Japan* **83**, 113708 (2014).
  - [2] Sai Swaroop Sunku, Tai Kong, Toshimitsu Ito, Paul C. Canfield, B. Sriram Shastry, Pinaki Sengupta, and Christos Panagopoulos, “Hysteretic magnetoresistance and unconventional anomalous hall effect in the frustrated magnet tmb<sub>4</sub>,” *Phys. Rev. B* **93**, 174408 (2016).
  - [3] Linda Ye, Takehito Suzuki, and Joseph G. Checkelsky, “Electronic transport on the shastry-sutherland lattice in ising-type rare-earth tetraborides,” *Phys. Rev. B* **95**, 174405 (2017).
  - [4] Hilbert v. Löhneysen, Achim Rosch, Matthias Vojta, and Peter Wölfle, “Fermi-liquid instabilities at magnetic quantum phase transitions,” *Rev. Mod. Phys.* **79**, 1015–1075 (2007).
  - [5] J. A. Mydosh and P. M. Oppeneer, “Colloquium: Hidden order, superconductivity, and magnetism: The unsolved case of uru<sub>2</sub>si<sub>2</sub>,” *Rev. Mod. Phys.* **83**, 1301–1322 (2011).
  - [6] W. Knafo, S. Araki, G. Lapertot, D. Aoki, G. Knebel, and D. Braithwaite, “Destabilization of hidden order in uru<sub>2</sub>si<sub>2</sub> under magnetic field and pressure,” *Nature Physics* **16**, 942–948 (2020).
  - [7] Christian Pfleiderer, “Superconducting phases of *f*-electron compounds,” *Rev. Mod. Phys.* **81**, 1551–1624 (2009).
  - [8] M. A. Ruderman and C. Kittel, “Indirect exchange coupling of nuclear magnetic moments by conduction electrons,” *Phys. Rev.* **96**, 99–102 (1954).
  - [9] Tadao Kasuya, “A theory of metallic ferro- and antiferromagnetism on zener’s model,” *Progress of Theoretical Physics* **16**, 45–57 (1956), <https://academic.oup.com/ptp/article-pdf/16/1/45/5266722/16-1-45.pdf>.
  - [10] Kei Yosida, “Magnetic properties of cu-mn alloys,” *Phys. Rev.* **106**, 893–898 (1957).
  - [11] D.J. Newman, “Theory of lanthanide crystal fields,” *Advances in Physics* **20**, 197–256 (1971).
  - [12] S. Shin, V. Pomjakushin, L. Keller, P. F. S. Rosa, U. Stuhr, C. Niedermayer, R. Sibille, S. Toth, J. Kim, H. Jang, S.-K. Son, H.-O. Lee, T. Shang, M. Medarde, E. D. Bauer, M. Kenzelmann, and T. Park, “Magnetic structure and crystalline electric field effects in the triangular antiferromagnet  $\text{CePtAl}_4\text{Ge}_2$ ,” *Phys. Rev. B* **101**, 224421 (2020).
  - [13] Jun Kondo, “Resistance minimum in dilute magnetic alloys,” *Nature Materials* **9**, 3324 (2018).

- [14] S. Seiro, L. Jiao, S. Kirchner, S. Hartmann, S. Friedemann, C. Krellner, C. Geibel, Q. Si, F. Steglich, and S. Wirth, “Evolution of the kondo lattice and non-fermi liquid excitations in a heavy-fermion metal,” *Nature Materials* **9**, 3324 (2018).
- [15] Shi-Zeng Lin and Cristian D. Batista, “Face centered cubic and hexagonal close packed skyrmion crystals in centrosymmetric magnets,” *Phys. Rev. Lett.* **120**, 077202 (2018).
- [16] Takashi Kurumajii, Taro Nakajima, Max Hirschberger, Akiko Kikkawa, Yuichi Yamasaki, Hajime Sagayama, Hironori Nakao, Yasujiro Taguchi Taka hisa Arima, and Yoshinori Tokura, “Skyrmion lattice with a giant topological hall effect in a frustrated triangular-lattice magnet,” *Science* **365**, 914–918 (2019).
- [17] Max Hirschberger, Taro Nakajima, Shang Gao, Li-cong Peng, Akiko Kikkawa, Takashi Kurumaji, Markus Kriener, Yuichi Yamasaki, Hajime Sagayama, Hironori Nakao, Kazuki Ohishi, Kazuhisa Kakurai, Yasujiro Taguchi, Xiuzhen Yu, Taka-hisa Arima, and Yoshinori Tokura, “Skyrmion phase and competing magnetic orders on a breathing kagome lattice,” *Nature Communications* **10**, 5831 (2019).
- [18] Ian A. Leahy, Keke Feng, Roei Dery, Ryan Baumbach, and Minhyea Lee, “Field-induced magnetic states in the metallic rare-earth layered triangular antiferromagnet  $\text{tbauAl}_4\text{Ge}_2$ ,” *Phys. Rev. B* **106**, 094426 (2022).
- [19] Kyle Fruhling, Alenna Streeter, Sougata Mardanya, Xiaoping Wang, Priya Baral, Oksana Zaharko, Igor I. Mazin, Sugata Chowdhury, William D. Ratcliff, and Fazel Tafti, “Topological hall effect induced by chiral fluctuations in  $\text{ermn}_6\text{sn}_6$ ,” *Phys. Rev. Mater.* **8**, 094411 (2024).
- [20] Motohiko Ezawa, “Giant skyrmions stabilized by dipole-dipole interactions in thin ferromagnetic films,” *Phys. Rev. Lett.* **105**, 197202 (2010).
- [21] N. S. Kiselev, A. N. Bogdanov, R. Schäfer, and U. K. Röbller, “Comment on “giant skyrmions stabilized by dipole-dipole interactions in thin ferromagnetic films”,” *Phys. Rev. Lett.* **107**, 179701 (2011).
- [22] Sebastian Mühlbauer, Benedikt Binz, F. Jonietz, Christian Pfleiderer, Achim Rosch, Anja Neubauer, Robert Georgii, and Peter Böni, “Skyrmion lattice in a chiral magnet,” *Science* **323**, 915–919 (2009).
- [23] X. Z. Yu, Y. Onose, N. Kanazawa, J. H. Park, J. H. Han, Y. Matsui, N. Nagaosa, and Y. Tokura, “Real-space observation of a two-dimensional skyrmion crystal,” *Nature* **465**, 901–904 (2010).
- [24] X. Z. Yu, N. Kanazawa, Y. Onose, K. Kimoto, W. Z. Zhang and S. Ishiwata, Y. Matsui, and Y. Tokura, “Near room-temperature formation of a skyrmion crystal in thin-films of the helimagnet  $\text{FeGe}$ ,” *Nature Materials* **10**, 106–109 (2011).
- [25] UK Röbller, AN Bogdanov, and C Pfleiderer, “Spontaneous skyrmion ground states in magnetic metals,” *Nature* **442**, 797–801 (2006).
- [26] Naoto Nagaosa and Yoshinori Tokura, “Topological properties and dynamics of magnetic skyrmions,” *Nature nanotechnology* **8**, 899–911 (2013).
- [27] F H De Leeuw, R Van Den Doel, and U Enz, “Dynamic properties of magnetic domain walls and magnetic bubbles,” *Reports on Progress in Physics* **43**, 689 (1980).
- [28] Yufan Li, N. Kanazawa, X. Z. Yu, A. Tsukazaki, M. Kawasaki, M. Ichikawa, X. F. Jin, F. Kagawa, and Y. Tokura, “Robust formation of skyrmions and topological hall effect anomaly in epitaxial thin films of  $\text{mnsi}$ ,” *Phys. Rev. Lett.* **110**, 117202 (2013).
- [29] Albert Fert, Vincent Cros, and João Sampaio, “Skyrmions on the track,” *Nature nanotechnology* **8**, 152–156 (2013).
- [30] R E Baumbach, T Shang, M Torrez, F Ronning, J D Thompson, and E D Bauer, “Local moment ferromagnetism in  $\text{CeRu}_2\text{Ga}_2$ ,” *Journal of Physics: Condensed Matter* **24**, 185702 (2012).
- [31] H. Sakai, Y. Tokunaga, S. Kambe, R. E. Baumbach, F. Ronning, E. D. Bauer, and J. D. Thompson, “Nmr study for  $4f$ -localized ferromagnet  $\text{CeRu}_2\text{Ga}_2$ ,” *Phys. Rev. B* **86**, 094402 (2012).
- [32] Eiichi Matsuoka, Yo Tomiyama, Hitoshi Sugawara, Takahiro Sakurai, and Hitoshi Ohta, “Ferromagnetic ground states with high transition temperatures in new tetragonal rare-earth compounds  $\text{CeRu}_2\text{Al}_2$  and  $\text{PrRu}_2\text{Al}_2$ ,” *Journal of the Physical Society of Japan* **81**, 043704 (2012), <https://doi.org/10.1143/JPSJ.81.043704>.
- [33] Dirk Wulferding, Hoon Kim, Ilkyu Yang, Juyoung Jeong, K Barros, Y Kato, I Martin, OE Ayala-Valenzuela, Minkyung Lee, Hee Cheul Choi, et al., “Domain engineering of the metastable domains in the  $4f$ -uniaxial-ferromagnet  $\text{CeRu}_2\text{Ga}_2$ ,” *Scientific reports* **7**, 46296 (2017).
- [34] Satoru Hayami and Yukitoshi Motome, “Néel- and bloch-type magnetic vortices in rashba metals,” *Phys. Rev. Lett.* **121**, 137202 (2018).
- [35] Minhyea Lee, W. Kang, Y. Onose, Y. Tokura, and N. P. Ong, “Unusual hall effect anomaly in  $\text{mnsi}$  under pressure,” *Phys. Rev. Lett.* **102**, 186601 (2009).
- [36] A Neubauer, C Pfleiderer, B Binz, A Rosch, R Ritz, PG Niklowitz, and P Böni, “Topological hall effect in the  $a$  phase of  $\text{mnsi}$ ,” *Physical review letters* **102**, 186602 (2009).
- [37] T Schulz, R Ritz, A Bauer, M Halder, M Wagner, C Franz, C Pfleiderer, K Everschor, M Garst, and A Rosch, “Emergent electrodynamics of skyrmions in a chiral magnet,” *Nature Physics* **8**, 301–304 (2012).
- [38] A. Bauer and C. Pfleiderer, “Magnetic phase diagram of  $\text{mnsi}$  inferred from magnetization and ac susceptibility,” *Phys. Rev. B* **85**, 214418 (2012).
- [39] A. Bauer, A. Chacon, M. Wagner, M. Halder, R. Georgii, A. Rosch, C. Pfleiderer, and M. Garst, “Symmetry breaking, slow relaxation dynamics, and topological defects at the field-induced helix reorientation in  $\text{mnsi}$ ,” *Phys. Rev. B* **95**, 024429 (2017).
- [40] A. Bauer, M. Garst, and C. Pfleiderer, “Specific heat of the skyrmion lattice phase and field-induced tricritical point in  $\text{mnsi}$ ,” *Phys. Rev. Lett.* **110**, 177207 (2013).
- [41] Peter E. Siegfried, Alexander C. Bornstein, Andrew C. Treglia, Thomas Wolf, and Minhyea Lee, “Multiple magnetic states within the  $a$  phase determined by field-orientation dependence of  $\text{mn}_{0.9}\text{Fe}_{0.1}\text{Si}$ ,” *Phys. Rev. B* **96**, 220410 (2017).
- [42] II Lobanova, VV Glushkov, NE Sluchanko, and SV Demishev, “Macroscopic evidence for abrikosov-type magnetic vortexes in  $\text{mnsi}$   $a$ -phase,” *Scientific Reports* **6**, 22101 (2016).
- [43] H Wilhelm, M Baenitz, M Schmidt, UK Röbller, AA Leonov, and AN Bogdanov, “Precursor phenomena at the magnetic ordering of the cubic helimagnet  $\text{FeGe}$ ,” *Physical review letters* **107**, 127203 (2011).



- [44] Lorenzo Vistoli, Wenbo Wang, Anke Sander, Qiuxiang Zhu, Blai Casals, Rafael Cicheler, Agnès Barthémy, Stéphane Fusil, Gervasi Herranz, Sergio Valencia, Radu Abrudan, Eugen Weschke, Kazuki Nakazawa, Hiroshi Kohno, Jacobo Santamaria, Weida Wu, Vincent Garcia, and Manuel Bibes, “Giant topological hall effect in correlated oxide thin films,” *Nature Physics* **15**, 67–72 (2019).
- [45] Masao Nakamura, Daisuke Morikawa, Xiuzhen Yu, Fumitaka Kagawa, Takahisa Arima, Yoshinori Tokura, and Masashi Kawasaki, “Emergence of topological hall effect in half-metallic manganite thin films by tuning perpendicular magnetic anisotropy,” *Journal of the Physical Society of Japan* **87**, 074704 (2018).
- [46] Davide Maccariello, William Legrand, Nicolas Reyren, Karin Garcia, Karim Bouzehouane, Sophie Collin, Vincent Cros, and Albert Fert, “Electrical detection of single magnetic skyrmions in metallic multilayers at room temperature,” *Nature Nanotechnology* **13**, 748–3395 (2018).
- [47] Juyoung Jeong, Ilkyu Yang, Jinho Yang, Oscar E. Ayala-Valenzuela, Dirk Wulferding, J.-S. Zhou, John B. Goodenough, Alex de Lozanne, J. F. Mitchell, Neliza Leon, Roman Movshovich, Yoon Hee Jeong, Han Woong Yeom, and Jeehoon Kim, “Magnetic domain tuning and the emergence of bubble domains in the bilayer manganite  $\text{La}_{2-2x}\text{Sr}_{1+2x}\text{Mn}_2\text{O}_7$  ( $x = 0.32$ ),” *Phys. Rev. B* **92**, 054426 (2015).
- [48] Jinho Yang, Ilkyu Yang, Yun Won Kim, Dongwoo Shin, Juyoung Jeong, Dirk Wulferding, Han Woong Yeom, and Jeehoon Kim, “Construction of a 3D magnetic force microscope with a vector magnet,” *Review of Scientific Instruments* **87**, 023704 (2016).
- [49] J. G. Checkelsky, Minhyea Lee, E. Morosan, R. J. Cava, and N. P. Ong, “Anomalous hall effect and magnetoresistance in the layered ferromagnet  $\text{Fe}_{1/4}\text{Ta}_{3/4}\text{S}_2$ : The inelastic regime,” *Phys. Rev. B* **77**, 014433 (2008).
- [50] Minhyea Lee, Y. Onose, Y. Tokura, and N. P. Ong, “Hidden constant in the anomalous hall effect of high-purity magnet mnsi,” *Phys. Rev. B* **75**, 172403 (2007).
- [51] SX Huang and CL Chien, “Extended skyrmion phase in epitaxial  $\text{Fe}_{111}$  thin films,” *Physical review letters* **108**, 267201 (2012).
- [52] Benjamin J. Chapman, Maxwell G. Grossnickle, Thomas Wolf, and Minhyea Lee, “Large enhancement of emergent magnetic fields in mnsi with impurities and pressure,” *Phys. Rev. B* **88**, 214406 (2013).
- [53] Naoto Nagaosa, Jairo Sinova, Shigeki Onoda, A. H. MacDonald, and N. P. Ong, “Anomalous hall effect,” *Rev. Mod. Phys.* **82**, 1539–1592 (2010).
- [54] N. Kanazawa, Y. Onose, T. Arima, D. Okuyama, K. Ohoyama, S. Wakimoto, K. Kakurai, S. Ishiwata, and Y. Tokura, “Large topological hall effect in a short-period helimagnet mng,” *Phys. Rev. Lett.* **106**, 156603 (2011).
- [55] Y. Shiomi, S. Iguchi, and Y. Tokura, “Emergence of topological hall effect from fanlike spin structure as modified by dzyaloshinsky-moriya interaction in mnp,” *Phys. Rev. B* **86**, 180404 (2012).
- [56] C. Franz, F. Freimuth, A. Bauer, R. Ritz, C. Schnarr, C. Duvinage, T. Adams, S. Blügel, A. Rosch, Y. Mokrousov, and C. Pfleiderer, “Real-space and reciprocal-space berry phases in the hall effect of  $\text{mn}_{1-x}\text{fe}_x\text{Si}$ ,” *Phys. Rev. Lett.* **112**, 186601 (2014).
- [57] L. J. Bannenberg, F. Weber, A. J. E. Lefering, T. Wolf, and C. Pappas, “Magnetization and ac susceptibility study of the cubic chiral magnet  $\text{mn}_{1-x}\text{fe}_x\text{Si}$ ,” *Phys. Rev. B* **98**, 184430 (2018).
- [58] Mark Maus, (2019), magnetic AC Susceptometry for Characterizing Magnetic Spin Structures, Undergraduate Honor Thesis, University of Colorado Boulder.
- [59] The area fraction is determined by dividing the centered MFM images into negative and positive force values, and subsequently calculating the ratio of the respective areas.
- [60] T. Shinjo, T. Okuno, R. Hassdorf, † K. Shigeto, and T. Ono, “Magnetic vortex core observation in circular dots of permalloy,” *Science* **289**, 930–932 (2000).
- [61] A. Wachowiak, J. Wiebe, M. Bode, O. Pietzsch, M. Morgenstern, and R. Wiesendanger, “Direct observation of internal spin structure of magnetic vortex cores,” *Science* **298**, 577–580 (2002).
- [62] K. Niitsu, T. Tanigaki, K. Harada, and D. Shindo, “Temperature dependence of  $180^\circ$  domain wall width in iron and nickel films analyzed using electron holography,” *Applied Physics Letters* **113**, 222407 (2018).
- [63] J. Raabe, R. Pulwey, R. Sattler, T. Schweinbk, J. Zweck, and D. Weiss, “Magnetization pattern of ferromagnetic nanodisks,” *Journal of Applied Physics* **88**, 4437–4439 (2000).
- [64] Brooke L. Mesler, Kristen S. Buchanan, Mi-Young Im, and Peter Fischer, “X-ray imaging of nonlinear resonant gyrotropic magnetic vortex core motion in circular permalloy disks,” *Journal of Applied Physics* **111**, 07D311 (2012).
- [65] Xiuzhen Yu, Akiko Kikkawa, Daisuke Morikawa, Kiyoyu Shibata, Yusuke Tokunaga, Yasujiro Taguchi, and Yoshinori Tokura, “Variation of skyrmion forms and their stability in mnsi thin plates,” *Phys. Rev. B* **91**, 054411 (2015).